Catalysis effect on the CO_2 methanation using MgH_2 as hydrogen portable medium

Received 00th January 20xx,
Accepted 00th January 20xx

DOI: 10.1039/x0xx00000x

Guillermina Amica[*a, b], Sara Rozas Azcona[c], Santiago Aparicio[c], Fabiana C. Gennari [a, b]

The feasibility of the reduction of CO_2 to CH_4 employing MgH_2 in the presence and absence of cobalt as catalyst was investigated for the first time, exploring different non-independent reaction conditions such as the grade of microstructural refinement, the molar ratio MgH_2:CO_2, reaction time and temperature. For the un-catalyzed process a methane yield of 44.6% was obtained after 24 h of thermal treatment at 400°C employing a molar ratio of 2:1, through a methanation mechanism that involves the direct reduction of CO_2 and the generation of CH_4 *via* C as an intermediary. For the MgH_2 catalyzed process a methane yield of 78% was achieved by heating at 350 °C for 48 h, being 4:1 the optimal molar ratio. The global mechanism responds to a Sabatier process favored by Co as an active catalyst, together with reversed water gas shift reaction followed by methanation of CO in presence of steam. On account of the fact that it was proved that the use of catalyst allows lowering the operational temperature without collapsing the methane yield, this research provides an interesting insight of a thermochemical method for CO_2 reduction to CH_4 employing a solid hydrogen storage medium as H_2 source.

1. INTRODUCTION

Since the industrial revolution, global economic growth has been sustained by low-cost energy production based on the exploitation of fossil resources, first coal and later natural gas and oil, as well as its derivatives. It is clear that the current energy system lacks sustainability as it faces problems of scarcity and dependence on hydrocarbons, non-renewable primary sources as well as unfriendly effects on the environment.[1] In fact, the global energy matrix based on the use of hydrocarbons has generated a strong environmental impact. The emission of greenhouse gases due to human activity, mainly carbon dioxide, has been responsible for the so-called climate change that includes not only global warming but also changes in rainfall, winds, in the cryosphere and level from sea. Greenhouse gases (GHG) emissions have risen at a rate of 1.5% per year in the last decade and reached a record high of 55.3 $GtCO_2e$ in 2018.[2] Fossil CO_2 emissions from energy use and industry, which dominates total GHG emissions, grew 2.0 per cent in 2018, reaching a record 37.5 $GtCO_2$ per year. Based on recent researches, specialists on the field have concluded that by 2030, emissions would need to be 25% and 55% lower than in 2018 to put the world on the least-cost pathway to limiting global warming to below 2°C and 1.5°C, respectively.[2] The strong growth in energy demand due to industrialization, the increase in urban population and improvements in the quality of life, along with the progressive depletion of fossil resources faces the world to a scenario of energy deficit. The technologies related to the capture and storage (CCS) and transformation of CO_2 into value-added products are attractive both from an environmental and economic point of view as it implies its reuse and recovery as a raw material.[3,4] Through various thermal or catalytic processes, CO_2 can be employed to synthesize a wide range of chemicals (urea, salicylic acid, carbonates, carboxylates, carbamates, acrylates, etc.) or different fuels (methane, methanol, olefins, etc.).[5-7] CO_2 conversion constitutes a promising alternative to employ a contaminant as a building block for fuels.

The methanation process, also known as Sabatier reaction, was first presented in 1902. It involves the combination of hydrogen with carbon dioxide at elevated temperatures and pressures in the presence of a catalyst to produce methane and water.[8] Recently, in the search of strategies that allow the storage of the excess renewable energy produced during peak generation periods, the study of this reaction has renewed relevance.[9-12] In this regard, Power-to-gas technologies seek the transformation of surplus renewable energy into a grid compatible gas, which can be used in future peak demand periods. Although this concept today cannot be achieved in a cost-effective manner, it offers the prospect of large-scale recycling CO_2 emissions, in combination with the use of renewable energy to form methane.[9] For example, instead of storing green H_2 produced via water electrolysis for later use as an energy vector in different applications, this H_2 can react with CO_2 through the Sabatier process to create methane, which can then be used on demand to generate electricity overcoming low points of renewable energy production.[10-15] The main advantage is that methane is a widely used fuel that has a large distribution infrastructure in many countries and it can be injected into the existing gas network, avoiding the challenges related to hydrogen

[a] *Consejo Nacional de Investigaciones Científicas y Técnicas (CONICET), Centro Atómico Bariloche (CNEA), Av. Bustillo 9500, R8402AGP +S.C. de Bariloche, Río Negro, Argentina*
[b] *Universidad Nacional de Cuyo (Instituto Balseiro), Centro Atómico Bariloche (CNEA), Av. Bustillo 9500, R8402AGP S.C. de Bariloche, Río Negro, Argentina*
[c] *Department of Chemistry, University of Burgos, Burgos, 09001, Spain*
† *Corresponding author: Guillermina Amica. guillerminaamica@gmail.com*

† Electronic Supplementary Information (ESI) available: Calculation procedure S1: Methane yield calculation procedure and numerical examples. Figure S1: Raman spectrum of MgH_2 after reaction with CO_2 (molar ratio of 2:1) at 400°C for 24 h. Figure S2: XRPD pattern of as milled sample and after thermal treatment (350°C, 24 h) under CO_2. Figure S3: Solid-state FTIR profiles for the as milled MgH_2-10%Co and after thermal treatment (400°C, 5 and 24h) under CO_2. Figure S4: Raman spectra of MgH_2-10%Co after reaction with CO_2 considering different experimental conditions. Figure S5: XRPD pattern of the sample MgH_2-10%wt Co with a molar ratio MgH_2:CO_2 of 4:1 (Co milled during the last 10 minutes). Figure S6: XRPD profile of the sample MgH_2-10%wt Co at 350°C with a molar ratio MgH_2:CO_2 of 2:1. Table S1: Gas-phase composition determined by gas chromatography analyses of the MgH_2-10wt % Co sample at 300°C. Figure S7: XRPD profile of the sample MgH_2-10%wt Co at 300°C with a molar ratio MgH_2:CO_2 of 4:1. Figure S8: Equilibrium composition (mol%) as a function of pressure at 450 °C for a molar ratio MgH2:CO2 of 4:1 (A) and 2:1 (B). Figure S9: Equilibrium composition (mol %) as a function of temperature at 1 bar for molar ratio MgH_2:CO_2 of 2:1. See DOI: 10.1039/x0xx00000x

storage. Through this strategy, renewable electric energy can be transformed into storable methane and CO_2 can be considered as an energy carrier for this process. In order to reach acceptable rate and selectivity for the methanation process, the use of appropriate catalysts is mandatory.[16-18] In fact, the lack of efficient and long-term operation catalysts limits its application in industrial scale.[18] This exothermic reaction (ΔH^{298K} = -165 kJmol^{-1}) typically operates between 200 and 450°C, depending on the catalyst and the experimental conditions (Reaction 1).[19,20] No general consensus exists on the reaction´s operating mechanism, mainly due to the uncertainty in determining the intermediate compound involved in the rate determining step. The discrepancy lies in the fact of considering the CO as an intermediary or not.[16]

$CO_{2(g)} + 4H_{2(g)} \rightarrow CH_{4(g)} + 2H_2O_{(g)}$ (ΔG^{298K} = -110 kJmol^{-1}) Reaction 1

Despite CO_2 methanation can be catalyzed by noble metals with high performance, the interest from an industrial view is limited due to their high costs and, instead, transition metals have been widely studied.[16] DFT calculations show spontaneous chemisorption of CO_2 on iron, cobalt, nickel and copper surfaces. It was demonstrated that the metal nature and its surface structure have a crucial role on the CO_2 chemisorption, affecting both the activation and the reduction steps involved in CO_2 hydrogenation.[17] Moreover, preservation and improvement of the metal activity can be achieved by selecting an appropriate support as they influence the activity, productivity and lifetime of the active phase.[16] The most usual supports are oxides (Al_2O_3, SiO_2, ZrO_2, TiO_2, CeO_2), zeolites, clays and mesoporous materials. The combination of the non-noble metal (one or several) with different supports, opens a range of catalyst behaviors due to the beneficial effects (or not) of the metal-support interaction.[18,21-28]

The reaction between hydrogen storage alloys with CO_2 was first explored in 1990. The oxidized surfaces allowed the generation of new carbonate species.[29,30] More recent studies showed that CO_2 can be reduced on the surface of hydrides that act as catalysts, by means of the Sabatier reaction allowing the conversion of CO_2 to methane and closing the cycle of carbon.[31-37] This allows the use of H_2 stored safely in a solid matrix (MHx, M: metal, H: hydrogen), which could acts as a catalyst for the transformation of CO_2 into a gaseous fuel. In particular, it was found that some complex hydrides such as, for example, Mg_2NiH_4, $Mg(BH_4)_2$, and $LiAlH_4$ possess good catalytic properties for the hydrogenation of CO_2, generating different chemical compounds of industrial interest.[31-35] Although the decomposition of alanates in atmospheres with CO_2 has been little explored, it is known that at temperatures greater than 120°C, $LiAlH_4$ reacts with CO_2, producing CH_4, H_2 and metal oxides.[32] Regarding borohydrides, the open structure of the gamma-$Mg(BH_4)_2$ phase and the high Mg^{2+} concentration make it an ideal material to be considered for CO_2 conversion, which occurs rapidly at low temperatures.[33] Through the study of the catalytic interactions of the surface of Mg_2NiH_4 with CO_2 during dehydrogenation, it was postulated that the dissociation of H_2 molecules on the surface is not the limiting step but adsorption dissociative of CO_2 molecules on the surface of the hydride.[31] The authors reported the formation of CH_4 and H_2O at 330 °C in the first cycle and, due to the formation of Ni nanoparticles that increase the catalytic activity of the system, it decreased to 280 °C in subsequent cycles.[31] Recently, the complex hydrides Mg_2FeH_6 and Mg_2NiH_4, prepared by a two-step procedure involving milling and sintering at high temperature, were proved to be good dual conversion promoters and hydrogen sources for the selectively CO_2 conversion to CH_4. It was revealed that the reversed water-gas shift reaction (WGSR) followed by the methanation of CO in the presence of steam dominates the process for the Mg_2FeH_6-CO_2 system, whereas for the Mg_2NiH_4-CO_2 system, the CO_2 direct reduction has a strong contribution.[34] Interestingly, it was proved that the synthesis method of Ni metal complex hydride has an impact on the global mechanism. Under the same experimental conditions, the methanation via as-milled Mg_2NiH_4 was proved to be faster and different from the one via as-sintered Mg_2NiH_4, with the presence of graphite in the solid phase.[35] In addition, recently, the thermochemical CO_2 reduction by alkali metal hydrides (LiH and NaH)[34] or alkaline-earth metal hydrides (CaH_2 and MgH_2)[35] in the absence of catalyst was presented. Both investigations agree that the yield of methane obtained depends strongly on the type of hydride, the H_2:CO_2 molar ratio and reaction conditions (temperature and time). The best performances were achieved by heat treatment at 450 °C for 48 h.[36,37] In that condition, methane yields were calculated to be 54.2, 68.0, 80.1 and 88.0 % employing NaH[36], MgH_2[37], LiH[36] and CaH_2[37], respectively.

In this work, for the first time the reduction of CO_2 to CH_4 using a hydride in the presence and absence of catalyst was investigated, allowing the study of different variables such as the microstructure, pressure, molar ratio H_2:CO_2, temperature and reaction times under the same conditions and using the same experimental set-up for the comparison between the un-catalyzed and catalyzed processes. Owing to the fact that our investigation group have previously explored the methane production *via* a catalytic process promoted by hydrides containing iron and nickel [34,35], in this work the use of cobalt was considered as this transition metal was also proved to have an excellent catalytic activity.[16,17,38] In particular, the feasibility of the use of MgH_2 for CO_2 conversion to CH_4, analyzing the role of cobalt as catalyst was investigated deeply and the reaction conditions that favor the desired products were explored. For the MgH_2 catalyzed process a methane yield of 78% was obtained by heat treatment at 350 °C for 48 h. This yield is not only considerably higher than the one previously reported at 350 °C (17 %) but, interestingly, it is also higher than that reported at 450 °C (68%).[37] Then, this research provides an interesting thermochemical method for CO_2 methanation employing a widely studied solid hydrogen storage medium (MgH_2) as H_2 source at lower temperatures.

2. EXPERIMENTAL

2.1 Materials preparation

The starting materials were commercial MgH_2 (Aldrich, 98%) and metallic Co (Aldrich, 99.9%). Due to the high reactivity of the samples, they were handled in a MBraunUnilab argon-filled glove box, with oxygen and moisture levels lower than 10 ppm. For all studies, high purity argon (Linde, 99.999%) was used. Two samples were prepared by mechanical milling (MM) in order to reduce particle size and achieve homogenous mixing: I) MgH_2 and II) MgH_2-10 wt% Co, using a sequence of 15 min milling and 10 min pause in

a planetary ball mill (Fritsch Pulverisette 6). Samples were ball milled during 5 h at 500 rpm with a ball to powder mass ratio of 53:1.

2.2 Characterization of the samples

The reaction between the samples and CO_2 was studied under flow and static conditions.

The dynamic measurements were performed in a TGA analyzer (TG-HP50, TA Instruments). In these experiments, the samples were heated at 5 °C.min^{-1} up to 400 °C in a continuous flow of CO_2. Additionally, the experiment was done using a flow of He to analyzed the decomposition of the sample in an inert atmosphere.

A stainless steel reactor coupled to a Sieverts volumetric equipment that allows the selection of the pressure and temperature was employed to study the reactivity under static conditions. A specific mass of each sample was introduced in the reactor inside the glove box to avoid contamination with oxygen or air humidity and then heated up with a ramp of 10 C.min^{-1} to different temperatures (300, 350 and 400°C) under CO_2 pressure. Two different molar ratios MgH_2:CO_2 were considered (4:1 or 2:1). The selected ratio, temperature and length of the thermal treatment are indicated in each experiment. The hydride amount was estimated taking into account the theoretical MgH_2 hydrogen storage capacity.

The composition of the gases after thermal treatment under CO_2 was studied employing gas-phase FTIR analyses (FTIR, Perkin Elmer Spectrum 400 with MCT detector) and gas chromatography (GC, Agilent Technologies GC System 7820A). For GC experiments 1 ml of the released gas was taken using a syringe, which was injected into the GC equipment. The molar amounts of gaseous CO_2, CH_4 and CO were quantified using calibration curves. Methane yield was calculated as: the ratio between the produced CH_4 moles and the total CO_2 moles at the beginning of the reaction (a numerical example is available at Supplementary Material). For IR spectroscopy measurements, the gases released were collected in a degassed quartz optical cell with KBr windows. The gas phase spectra at room temperature were taken with a resolution of 0.5 cm^{-1}.

The structural and thermal properties of the as-milled and after thermal treatment under CO_2 solid samples were studied using X-ray powder diffraction (XRPD, DRX Bruker D8 Advance), Fourier transform infrared spectroscopy (FTIR, Perkin Elmer Spectrum 400 with MCT detector) and Raman spectroscopy (LabRAM HR Evolution Raman microscopy). During the XRPD data collection, all the samples were kept under an Ar atmosphere using an airtight holder, which has a bump in the zone of 2Θ=15-25°, to prevent any reaction between samples and air. For IR spectroscopy measurements, the samples were ground with dry KBr under a purified argon atmosphere, pressed to pellets and placed in a specially designed airtight cell. Handling was done inside the glove box to avoid contact with air. Solid state IR spectra were obtained in the range of 4000–800 cm^{-1} with a resolution of 4 cm^{-1}. Raman spectroscopy was employed to analyze the solid samples after treatment under CO_2 in order to identify carbon and carbon compounds at room temperature and using a laser wavelength of 514 nm. Morphological and agglomerate size distribution analyses of the samples were performed by Scanning electron microscopy (SEM, SEM-FIB, Zeiss, Crossbeam 340), employing dispersed powders a carbon tape. Elemental analyses of the materials were also performed by energy-dispersive X-ray spectroscopy (EDXS) on SEM.

2.3 Thermodynamic calculations

The equilibrium compositions for the MgH_2–CO_2 system as a function of the temperature and also as a function of pressure were calculated using HSC Chemistry Windows.[39] Given all the species (reactants and products) in a reaction system, the software determines the distribution of the products where the Gibbs free energy of the system reaches its minimum. The calculation was conducted based on gas phase containing CO_2, H_2, CO, CH_4, H_2O, C_2H_4, C_2H_6 and CH_3OH and solid phase containing Mg, MgO, $Mg(OH)_2$, $MgCO_3$, MgC_2, Mg_2C_3 and C.

3. RESULTS

3.1 CO_2 conversion in the presence of MgH_2 without catalyst.

To investigate the conversion of CO_2 in the presence of MgH_2 without any catalyst addition, the as- milled hydride was heated up to 400°C in static conditions under a CO_2 atmosphere during 24 h. Two different molar ratios MgH_2:CO_2 were considered (4:1 and 2:1) in order to evaluate its influence on the product formed and further elucidate the reaction mechanism. Ball milling was employed to activate the commercial MgH_2, as it is expected that its reactivity increases with microstructure refinement. This effect can be associated to both the agglomerate size reduction and the crystallite size reduction. The bigger exposed area available for the reaction is responsible for the increase in reactivity.

The evolution of the phases due to the interaction with CO_2 was studied by XRPD and FTIR (Fig. 1). Although the XRPD profile of the as-milled MgH_2 reveals a low crystallinity after milling, the absence of impurities was confirmed (Fig. 1A). The broad and weak diffraction peaks show that mechanical milling was effective in reducing strongly the particle size. After thermal treatment under CO_2, for both, the 4:1 and the 2:1 samples, Mg and MgO were easily detected. The main difference is that, for the former, unreacted MgH_2 was identified. In addition, solid-state FTIR revealed that for the 4:1 sample no carbonate phases were formed and the presence of unreacted MgH_2 cannot be discarded (Fig. 1B). On the other hand, for the 2:1 sample no MgH_2 was detected, whereas some bands at the band region 1600–600 cm^{-1} could be related to the presence of carbonates favored by the higher CO_2 pressure.[40,41] Among them, the bands located at 1063, 879 and 1415 cm^{-1} could be attributed to the vibration modes (v1, v2 and v3, respectively) of superficial carbonate species on MgO.[40] For MgH_2, stretching bands consists in various peaks with the strongest one at 1246 cm^{-1} and the bending band at 658 cm^{-1}.[42]

The presence of elemental C (bands G and D) and carbonates was confirmed by Raman measurements (see Fig. S1).

As shown in the SEM images (Fig. 2), the morphological characteristic of the as-milled MgH_2 agglomerates is its spongy form and its wide size agglomerate distribution between 5 and 50 microns.

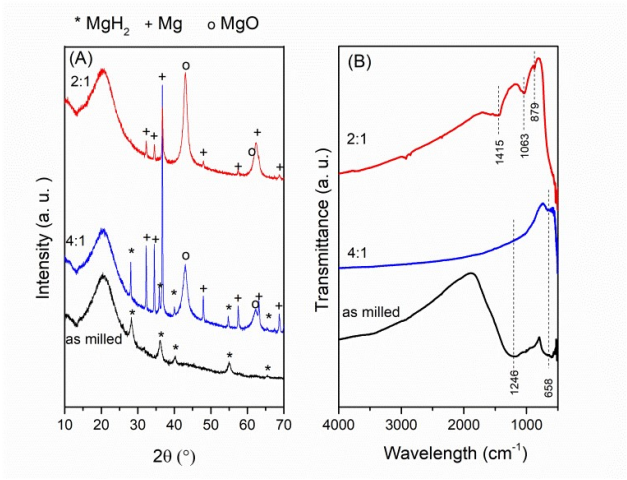

Figure 1: XRPD patterns (A) and solid-state FTIR spectra (B) of as-milled sample and after thermal treatment (400°C, 24 h) under CO_2.

After thermal treatment under CO_2, the sample is composed of micrometric agglomerates with appreciable amount of pores.

The average agglomerate size increased by treatment at 400° C. Previous studies[34] in similar materials have revealed that the spherical particles correspond to MgO formed due to the CO_2 reduction in presence of MgH_2 (some of them are indicated in Fig 2D). Regarding the surface morphology, before the reaction, particles with straight edges were detected, while after the reaction all the particles are small and rounded, with round MgO particles.

The gas-state products of the reaction between MgH_2 and CO_2 were identified and quantified by gas chromatography. Clear H_2 and CH_4 chromatography's peaks were observed. An excess of CO_2 and co-generation of minor percent of CO were also detected in some cases (see Table 1).

Increasing the CO_2 proportion elevates the mole percentage of CH_4 from 17.8 (relation 4:1) up to 46.4 (relation 2:1) after 24 h at 400°C.

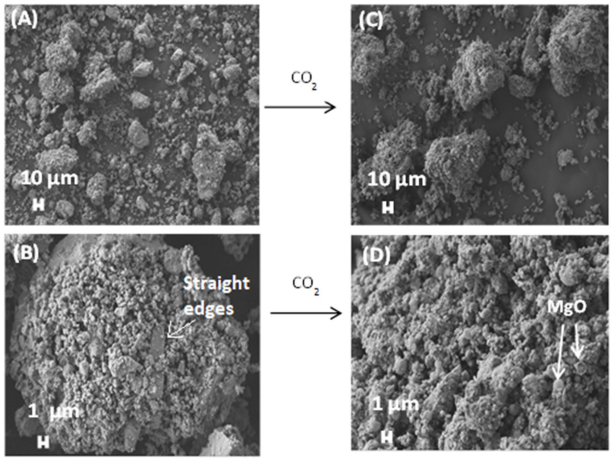

Figure 2: SEM images of the as-milled MgH_2 (A, B) and after thermal treatment under CO_2 (C, D).

Moreover FTIR analyses of the resulting gas phase after reaction with CO_2 at 400°C, considering a molar ratio of 2:1, were performed to prove the presence or absence of H_2O. In Figure 3 the patterns for 5 and 24 h are compared. Although GC experiments revealed the presence of a small amount of CO_2 and CO after 24 h (see Table 1), these species are not detected by this technique as the quantity is below the detection limit. As expected, when reaction time was increased, CO_2 is consumed and the bands corresponding to CO are no longer identified. The presence of H_2O is not unequivocally established. The presence of higher hydrocarbons such as ethane or propane (C_xH_y) is suspected due to the weak absorption peaks at 1470 and 2968 cm^{-1}.[36,43]

In order to analyze the role of temperature, the sample was thermal treated under CO_2 (with a relation MgH_2:CO_2 of 2:1) at a lower temperature: 350°C instead of 400°C. The reaction yield drops drastically from 44.9% at 400°C to 0.4% at 350°C (see Table 1). XRPD analysis shows that the solid sample is mainly composed of unreacted MgH_2, whereas Mg and MgO can also be identified (see Fig S2). Although MgH_2 can be decomposed under certain backpressure of an inert gas at temperatures lower than 400°C, this observation indicates that the presence of CO_2 inhibits its decomposition. For the set of experiments performed, the best results were obtained for a thermal treatment of 24 h at 400°C considering a ratio MgH_2:CO_2 of 2:1. As show in Fig. 1, for this sample no MgH_2 remains in the solid product, which means that the experimental conditions allowed the complete decomposition of the reactant.

3.2 CO_2 conversion in the presence of MgH_2 with Cobalt as catalyst.

3.2.1. Characterization of the as-milled sample

The as-milled doped sample MgH_2-10wt%Co was analyzed by XRPD (Fig. 4). As expected, it is composed of MgH_2 and metallic Co (2Θ= 41.7, 44.8, 47.6°) and no other Co-containing compounds were formed due to mechanical milling. SEM images of the sample after ball milling showed that the average agglomerate size was not modified by the presence of Co (~ 40 µm) and the element mapping obtained by EDXS indicates homogeneous distribution of Co (Fig. 5).

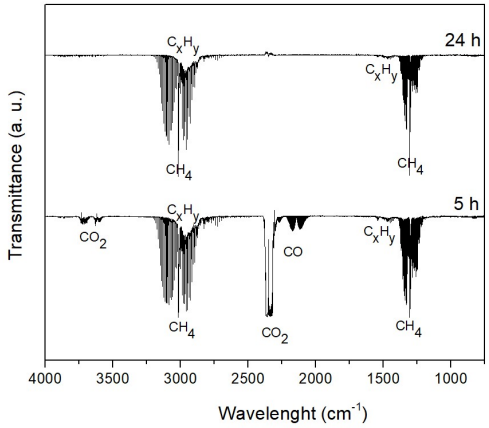

Figure 3: Gas-state FTIR patterns for the as-milled sample after thermal treatment under CO_2 (2:1) at 400 °C for 5 h (as-reacted) and 24 h (after dilution).

Table 1: Gas-phase composition determined by gas chromatography analyses for as-milled MgH_2.

Temperature (°C)	MgH_2:CO_2	Reaction time (h)	Molar percentage of CH_4 (%)	Molar percentage of CO_2 (%)	Molar percentage of CO (%)	Molar percentage of H_2 (%)	CH_4 yield (%)
400	4:1	24 h	17.8	0.6	0	81.6	42.4
400	2:1	5 h	6.8	37.9	6.8	48.5	4.3
400	2:1	24 h	46.4	0.9	<1000 ppm	52.7	44.6
350	2:1	24h	3.8	67.5	5.2	23.5	0.3

3.2.2 Reactivity of MgH_2 with CO_2 under dynamic conditions

The carbon dioxide absorption of MgH_2 and MgH_2-10wt% Co after ball milling for 5 h was first studied and compared under dynamic conditions by thermogravimetry (Fig.6).

Dehydrogenation temperature of the as-milled samples was analyzed using TG in He flow with a heating ramp of 5°C/min. The decomposition reaction of the doped and un-doped MgH_2 displayed a one-step dehydrogenation process with a big difference on the temperature at which decomposition begins. TG measurements revealed that the dehydrogenation temperature of MgH_2 (330°C) was lowered ~80°C by the addition of Co (estimated at 0.1% of mass change).

Regarding the hydrogen content, at 400°C MgH_2 released 7.3 wt% H_2, which represents the 96% of its theoretical capacity (7.6 wt% H_2). Hence, the decomposition of MgH_2 under inert gas flow can be represented by Reaction 2.

MgH_2 (s) → Mg (s) + H_2 (g) Reaction 2

As expected, the addition of Co induced a drop in the hydrogen capacity. 6.2 wt% H_2 was released, whereas the expected theoretical value considering the amount of dopant is f 6.8 wt% H_2.

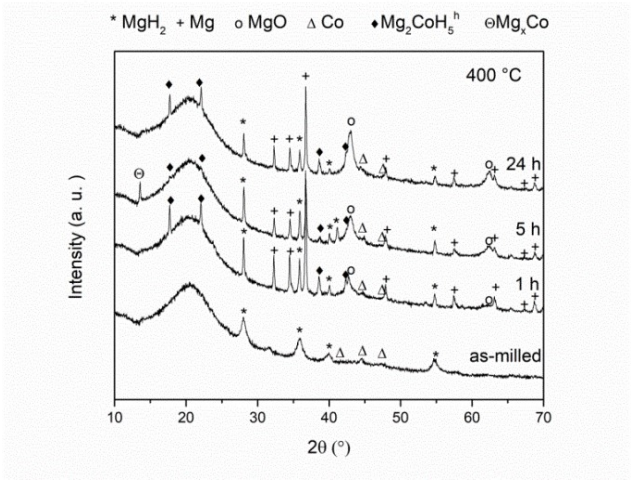

Figure 4: XRPD patterns of the as-milled and after thermal treatment under CO_2 at 400°C of the MgH_2-10wt% Co sample.

On the other hand, thermogravimetric results show that when both samples are exposed to a CO_2 flux from room temperature up to 400 °C, mainly mass gain is observed (Fig. 6).

The weight increase does not change considerably when Co is incorporated by ball milling. In fact mass change is of about 12% in both cases, with a slight mass loss near 400 °C.

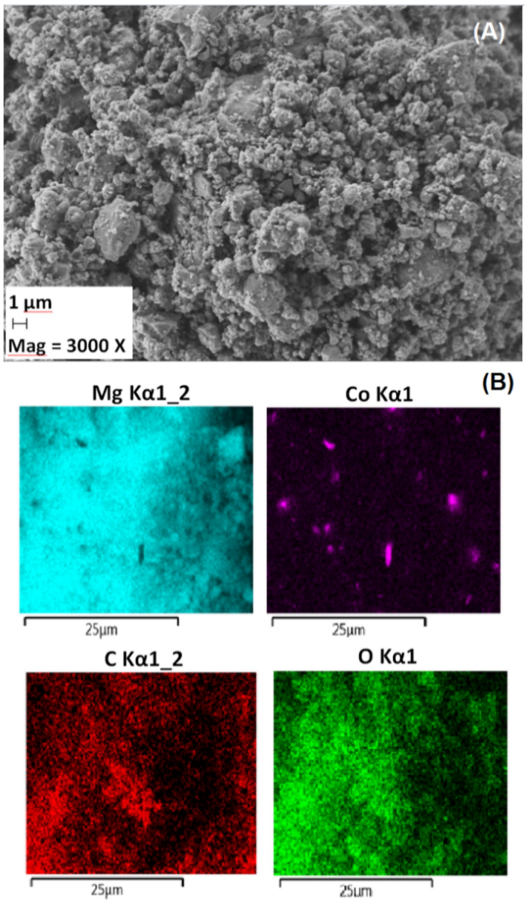

Figure 5: (A) SEM images of secondary electron; (B) Elemental mapping of the as-milled MgH_2-10wt% Co sample.

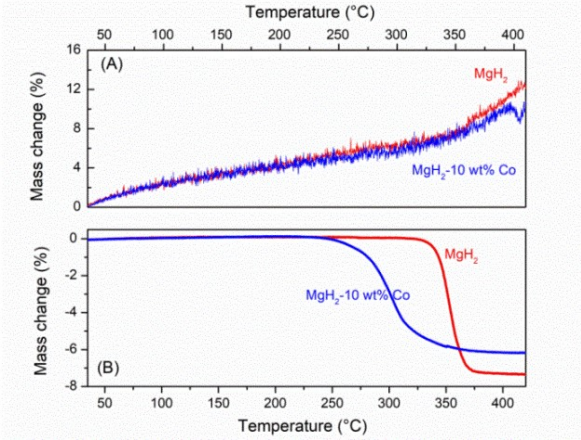

Figure 6: Thermogravimetric measurements of the MgH_2 and MgH_2-10wt%Co samples under CO_2 (A) and He (B).

It has been already demonstrated that for certain hydrides studied, the initial CO_2 absorption induces only mass gain and retard the dehydrogenation by passivation or oxidation of the hydride surface.[31,34] This means H_2 is released at higher temperatures when the hydride is exposed to a CO_2 flux respect to an inert gas flow.

3.2.3 Reactivity of catalyzed MgH_2 with CO_2 under Static conditions

To investigate the conversion of CO_2 in the presence of catalyzed MgH_2 after milling by heating in static conditions, different temperatures and durations of thermal treatment were employed. Unless otherwise stated, in all cases MgH_2:CO_2 ratio of 4:1 was considered.

GC analyses were performed to analyze the gas phase obtained after reaction at 400°C, varying the duration of the thermal treatment: 1, 5 and 24 h. It was observed that when reaction time was increased, the gas phase was richer in CH_4 and poorer in CO_2 and CO (see Table 2). Notably, for 24 h a CH_4 yield of 60.9 % was reached.

The obtained solid products after thermal treatment under CO_2 were analyzed by XRPD (see Fig. 4). In the three XRPD patterns Mg, MgO and MgH_2 are easily identified. Moreover, the presence of small peaks corresponding to metallic Co cannot be discarded. Interestingly after 1 h of thermal treatment the complex mixed Co and Mg hydride with hexagonal structure ($Mg_2CoH_5^h$) was formed and after 24 h it was still detected. However, at an intermediate time, Mg_2CoH_5 is hardly observed but an intermetallic compound, identified by its most intense peak at 2Θ=13.4°, which corresponds to Mg_xCo was identified.[44] In literature there are two different reported processes through which this intermetallic compound can be formed: 1) Diffusion in solid state of Mg and Co powders during thermal treatment or 2) Hydrides (Mg_2CoH_5 or $Mg_6Co_2H_{11}$) decomposition. When MgCo is exposed to heat treatment in the presence of H_2 and free Mg, Mg_2CoH_5 can be formed according to: $MgCo(s) + Mg(s) + 5/2H_2(g) \rightarrow Mg_2CoH_5(s)$.[45] Then, the coexistence of metallic Co and a co-formed phase such as Mg_2CoH_5 or Mg_xCo may have a catalytic role.[45] Solid-state FTIR analyses proved the presence of carbonate species by the identification of two bands located at 1063 and 1260 cm^{-1} which correspond to carbonate unidentate and bidentate, respectively, on MgO (see Fig. S3).[40,41] Raman measurements of the obtained solid samples allowed discarding the presence of elemental C (see Fig. S4).

Seeking to disfavor the formation of Co-containing compounds in order to have available metallic cobalt, a new sample in which the Co was incorporated to the MgH_2 at the end of the ball milling (during the last 10 minutes) was prepared. As an unexpected result, after thermal treatment under CO_2 for 5 h (denoted in Table 2 as 5h*), similar results were obtained. The complex hydride is not formed, metallic Co is identified and the peak corresponding to the intermetallic is incipient, which means that even in this case Co reacts to form Mg_xCo (see Fig S5). Thus, the addition of Co at the end of the milling processing did not have a major effect on the CH_4 yield. Considering the set of experiments presented in Table 2, unlike what was observed for the sample without catalyst, there are no major differences when increasing the heat treatment time from 5 to 24 hours at 400°C. For the 24h-treated sample, in addition to CH_4, the presence of H_2O was confirmed by gas-phase FTIR and CO_2 and CO were not detected as the quantity is below the detection limit (see Fig. 7). Moreover, the presence of superior hydrocarbons is discarded.

SEM images of the sample after 5 h of thermal treatment under CO_2 showed the existence of micrometric agglomerates with a great amount of pores (Fig. 8). The element mapping obtained by EDXS shows a homogenous distribution of Co. Although some rounded particles (MgO) were identified, the amount is lower than the observed for the sample without additive.

The viability of the CO_2 hydrogenation was analyzed at 350°C. At this temperature the reaction length was crucial. Unlike what was conditions, the gas phase was mainly composed of CH_4 (49.7 mol%) and H_2, with a little excess of CO_2 (0.5mol%) and reaction yield increase up to 78%.

XRPD measurements obtained after CO_2 conversion at 350 °C (Fig. 9) showed that as the reaction time increases, the amount of MgH_2 decreases markedly, while the amount of Mg and MgO increases. At this temperature, after 5 h only the tetragonal phase of Mg_2CoH_5 was detected ($Mg_2CoH_5^t$). At higher reaction times there is a structural phase transition, the tetragonal phase was hardly visible but the peaks corresponding to hexagonal Mg_2CoH_5 appeared.

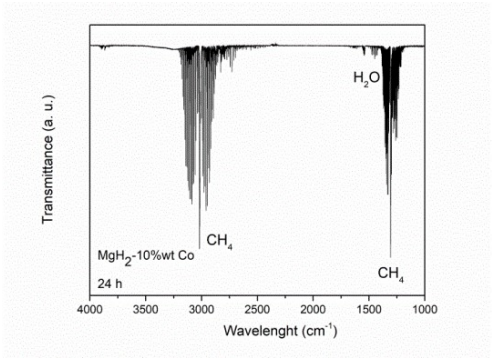

Figure 7: Gas-phase FTIR profile for the MgH_2-10wt%Co after thermal treatment (400°C, 24h) under CO_2.

Table 2: Gas-phase composition determined by gas chromatography analyses of the MgH_2-10wt %Co sample at 400°C.

Reaction time (h)	Molar percentage of CH_4 (%)	Molar percentage of CO_2 (%)	Molar percentage of CO (%)	Molar percentage of H_2 (%)	CH_4 yield (%)
1	6.3	21.8	0.1	71.8	15
5	34.2	7.7	0.2	57.9	57.1
5 *	32	9	0.1	58.9	61.3
24	38.2	0.8	<1000 ppm	61	60.9

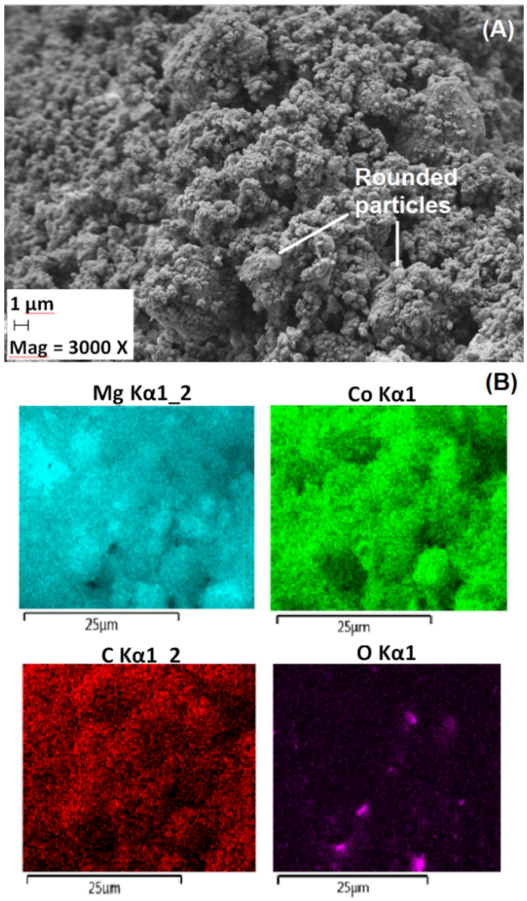

Figure 8: (A) SEM images of secondary electron; (B) Elemental mapping of the MgH_2-10wt%Co sample after thermal treatment (400°C, 5 h) under CO_2.

Moreover the experiment was repeated considering a molar ratio MgH_2:CO_2 of 2:1 instead of 4:1 (24 h at 350 °C). Although the percentage of methane grew, a big amount of CO_2 remained unreacted and CO was generated (see Table 3). This was reflected in the calculated methane yield (27.6%). The XRPD analyses of the solid product (Fig. S6) revealed the presence of unreacted MgH_2, as well as MgO, Mg_2CoH_5 (tetragonal and hexagonal phases) and metallic Co. Metallic Mg was hardly observed, which indicates that the majority was oxidized.

Motivated by the good results at 350°C, reaction temperature was further decreased to 300°C. However poor results were obtained (CH_4 yield <1%) (see Table S1). Most of the CO_2 remained unreacted and CO was considerably generated. Consistently, the XRPD pattern of the obtained solid sample showed a big amount of unreacted MgH_2. Mg was identified but no MgO was detected. Metallic Co is clearly identified and there are incipient peaks related to tetragonal Mg_2CoH_5 (see Fig. S7).

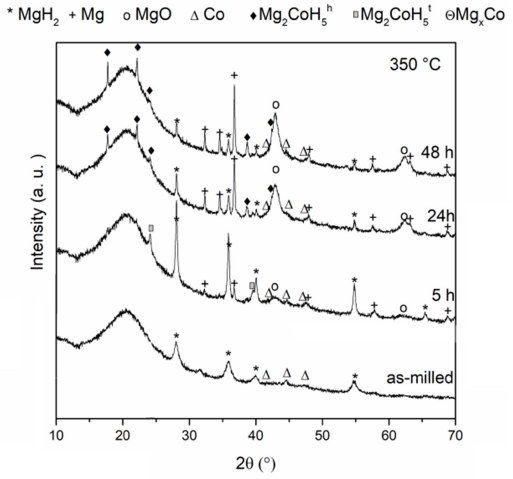

Figure 9: XRPD profiles of the as-milled MgH_2-10wt% Co sample and after thermal treatment at 350°C under CO_2.

Table 3: Gas-phase composition determined by gas chromatography analyses of the MgH_2-10wt%Co sample at 350°C

MgH_2:CO_2	Reaction time (h)	Molar percentage of CH_4 (%)	Molar percentage of CO_2 (%)	Molar percentage of CO (%)	Molar percentage of H_2 (%)	CH_4 yield (%)
4:1	5	3.1	62.9	18.6	15.4	3.4
	24	42.3	0.6	<1000 ppm	57.1	59.7
	48	49.7	0.5	-	49.8	78
2:1	24	50.2	35	13	1.8	27.6

4. DISCUSSION

The methanation mechanism is a complex process which depends on several factors: on the one hand it depends on the presence of catalyst and its nature and on the other, on the grade of microstructural refinement (in this case, provided by mechanical activation), reaction temperature and time. The calculated methane yields are represented in Figure 10. Moreover, Figure 11 displays a summary of the GC results, showing the molar fractions of both the CO_2 remained in excess and the generated CH_4 after thermal treatment in different operational conditions.

From figure 10, it can be observed that without catalyst a methane yield of 44.6% can be obtained after 24 h of thermal treatment at 400°C employing a molar ratio MgH_2:CO_2 of 2:1. In this condition, the gas phase is composed of 46.4 % of CH_4 with an excess of CO_2 of 0.9 % and a small amount of generated CO (<1000 ppm) (see Fig. 10). The presence of a small amount of superior hydrocarbons (ethane or propane) was proved by gas state FTIR (see Fig. 3). The solid product was demonstrated to be composed of Mg and MgO and no MgH_2 remained unreacted. Carbonate species were detected by solid state-FTIR (see Fig. 1B). Moreover the presence of C and carbonates was confirmed by FTIR and Raman measurements (see Fig. 1 and S1). When either the temperature or the reaction time is lowered, the performance values drop sharply and, logically, it is accompanied by a decrease in the amount of CH_4 and an increase in the amount of CO_2, with the clear identification of CO (around 6%) (see Fig. 11).

In order to understand the methanation mechanism that explain this process, Gibbs free energy minimization method was employed to predict the distribution of the products in both the solid and gas phase at chemical equilibrium for reaction between MgH_2 and CO_2. This represents the expected reaction without the use of any catalyst. The mole fraction of the products (%) was obtained as a function of CO_2 pressure at 400°C for a molar ratio MgH_2:CO_2 of 4:1 (Fig. 12 A) and 2:1 (Fig. 12B).

From these calculations, it can be inferred that the molar ratio MgH_2:CO_2 has an influence on the equilibrium composition of the system.

Regarding the gas phase for the relation 4:1, it is expected to be richer in H_2 than in CH_4, whereas for the relation 2:1 the opposite occurs. In both cases no residual CO_2 or CO formation is expected. For the latter case, the amount of CH_4 produced increases more strongly with pressure. Moreover there are differences in the composition of the solid. While for the relation 4:1 part of the MgH_2 does not react, when the relation 2:1 is considered, only MgO and C are identified as solid products and no MgH_2 is expected. Experimentally, it was determined that the interaction between the CO_2 that reaches the solid surface of the sample and the H_2 released from the hydride depends strongly on the molar ratio between MgH_2 and CO_2.

Comparing Figure 12 A and B, it is clear that employing a relation 2:1 favors the CH_4 production when no catalyst is added. The experimental results obtained at 400°C (see Table 1) are consistent with the above presented observations. In addition, the same thermodynamic analysis was performed at 450°C (see Fig. S8). Notably, with a 2:1 ratio, if temperature rises from 400 to 450 °C, the amount of CH_4 decreases for a determined pressure, suggesting that this experimental condition is not favorable.

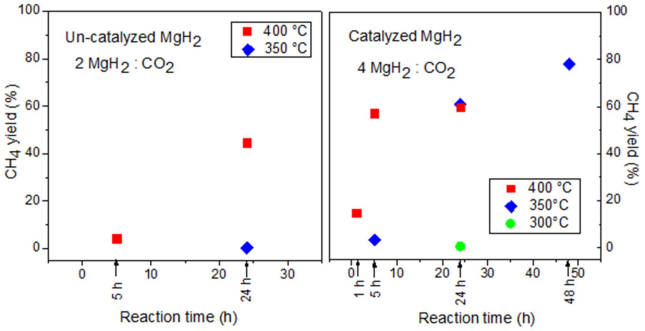

Figure 10: Methane yields (%) obtained after reaction with under CO_2 at different temperatures and reaction times (h).

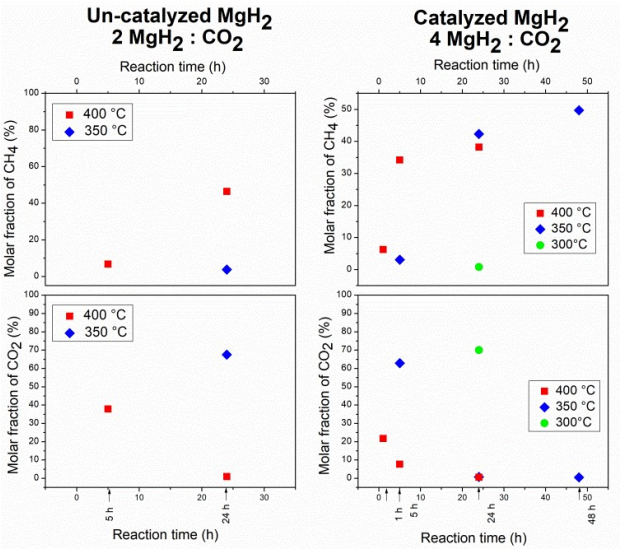

Figure 11: Molar fraction (%) of CH_4 and CO_2 obtained at different temperatures (°C) and reaction times (h) after reaction with CO_2 for the un-catalyzed and catalyzed samples.

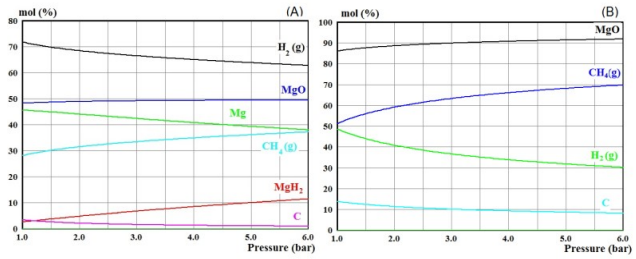

Figure 12: Equilibrium composition (mol%) as a function of pressure at 400 °C for a molar ratio MgH_2:CO_2 of 4:1 (A) and 2:1 (B).

While this seems opposite to previous observations, the kinetics may be favored at higher temperatures.[37] From a thermodynamic point of view, considering a constant pressure of 1 bar, to obtain high CH_4 yield and avoid carbon deposition it is desirable to operate the system at low temperatures (<75°C) because if temperature rises, a mixture of CH_4 and H_2 is obtained (see Fig. S9). However, previous experiments have shown good results exploring the feasibility of conversion at high temperatures (450-500°C).[36-37] Moreover, it was demonstrated that is not possible to lower the reaction temperature without affecting the molar percentage of CH_4 considerably. When the reaction temperature is lowered from 400 to 350°C, the reaction does not progress as expected (see Table 1). The experimental amount obtained of the desired gas product (CH_4) at 400 °C after treatment of 24 h (46.4 %) was lower than that predicted by the thermodynamic estimations (60%). The difference is attributable to kinetic restrictions and the availability of carbon surface to react with H_2.

Considering the information presented above, a global mechanism for the direct reduction of CO_2 by MgH_2 without catalyst (also called CO_2 hydrogenation), for a molar ratio MgH_2:CO_2 of 2:1, can be proposed involving reactions 3 and 4. The enthalpy of Reaction 3 is negative in the entire temperature range from ambient onwards and as the temperature rises, it becomes more negative. On the other hand, for Reaction 4, when temperature increases, the enthalpy is less negative and becomes positive for temperatures over 500°C. That is the reason why CH_4 and H_2 always coexist in the gas phase resultant from these samples and it is not possible to obtain pure CH_4. The thermodynamic calculations predict that reactions 3 and 4 occur simultaneous, changing the relative amounts of coexistent species (C, MgO, CH_4 and H_2) as a function of pressure.

$2MgH_2(s) + CO_2(g) \leftrightarrow 2MgO(s) + 2\ H_2(g) + C(s)$ Reaction 3

$C(s) + 2\ H_2(g) \leftrightarrow CH_4(g)$ Reaction 4

Additionally, when equilibrium is not reached, CO_2 is not totally reduced to C, but it is partially reduced to CO. This explains the presence of CO for short reaction times or low temperatures. In this case, Reaction 5 and Reaction 6 occur in series, with CO as an intermediate in the reduction of CO_2 to carbon. If both reactions are added, the previously proposed Reaction 3 is obtained. Moreover, the detection of small amounts of $MgCO_3$ can be justified by the magnesium oxide carbonation by reaction with CO_2, whereas, the generated CO can be consumed to form superior hydrocarbons through a Fischer–Tropsch reaction or other products through different reactions.[46]

$MgH_2(s) + CO_2(g) \leftrightarrow MgO(s) + H_2(g) + CO(g)$ Reaction 5

$MgH_2(s) + CO(g) \leftrightarrow MgO(s) + C(s) + H_2(g)$ Reaction 6

The use of catalysts allows the methanation mechanism to be different from the one described above. From Fig. 10 it can be point out that, for a 24 h-treatment of the cobalt-catalyzed MgH_2, it is possible to lower the operational temperature from 400 to 350°C without collapsing the methane yield but a temperature of 300°C is not enough to achieve reasonable conversions. On the other hand, reducing the duration of the reaction to 5h is only feasible at 400°C. The best methane yield (78%) was obtained for the MgH_2-10 wt% Co sample per treatment under CO_2 for 48 hours at 350°C considering a molar ratio MgH_2:CO_2 of 4:1 (see Fig. 10). In this condition the gas phase contained 49.7% CH_4 with CO_2 in excess of 0.5% (see Fig. 11). After 24 h of thermal treatment, the gas phase was composed by a mixture of CH_4 (46.4%) and H_2 (52.9%), with a small amount of unreacted CO_2 (0.9%) and practically none CO (<1000 ppm) (see Table 1). The catalyzed process is highly selective to methane, as there was no evidence of the formation of other hydrocarbons such as ethane or propane (see Fig. 7). Then, at 350°C, the longer the time reaction, the more favored the CO_2 conversion is. These observations indicate that even with the use of catalyst, the selection of the appropriate temperature and time reaction is crucial as there is a compromise between these two non-independent parameters. Considering all the experimental evidence, it can be proposed that the process for the MgH_2 catalyzed sample occurs via *Sabatier reaction* according to the global Reaction 7, after MgH_2 decomposition into Mg and H_2 trough Reaction 2. This process is favored by active catalysts such as Co. According to the stoichiometry of this reaction, the required molar ratio between MgH_2 and CO_2 is 4:1. Metallic Mg can be oxidized by reaction with CO_2 according to Reaction 8.

$MgH_2 \leftrightarrow Mg + H_2$ Reaction 2
$CO_2 + 4H_2 \leftrightarrow CH_4 + 2\ H_2O$ Reaction 7
$Mg + CO_2 \leftrightarrow MgO + CO$ Reaction 8

The presence of water detected by gas-phase FTIR experiments is strong evidence indicating that the methanation process takes place through the proposed mechanism. Moreover, when the molar ratio MgH_2:CO_2 was changed from 4:1 to 2:1, the methanation performance was worsened. CO co-generated could not be avoided and a big amount of CO_2 remained unreacted (see Table 3). The difference observed respect to the previous results might indicate that the system is disproportioned. Although hydrogen remained in the solid, both in MgH_2 and Mg_2CoH_5, the amount of CO_2 is high and limits the release of H_2 from the hydrides. This limitation may be from a kinetic nature, due to surface passivation as the CO is chemisorbed onto cobalt. Then, unlike what was demonstrated for the un-catalyzed system, in this case the optimal molar ratio is 4:1. These two characteristics confirm that the global process of CO_2 reduction by catalysed MgH_2 with Co responds to a *Sabatier process*. It has been previously demonstrated that at 1 bar the CH_4 selectivity and CO_2 conversion are optimized at low temperatures and that although the reaction rate increases with temperature, the formation of CO by-product is favored above 450 °C due to reversed water gas shift reaction (Reaction 9).[34] However, depending on the specific catalysis mechanism, the presence of CO can be detected at lower temperatures. CO formation was observed at short reaction times or low temperatures (see Table 3), but, for longer reaction times it is consumed trough reaction with H_2 to generate more CH_4 (Reaction 10). MgH_2 was always identified in the solid phase which means that part of H_2 was retained in the hydride phase, inhibiting to achieve higher conversion rates.

$CO_2+H_2 \leftrightarrow CO+H_2O$ Reaction 9
$CO+3H_2 \leftrightarrow CH_4 + H_2O$ Reaction 10

5. CONCLUSIONS

In this work, for the first time, the feasibility of the reduction of CO_2 to CH_4 using MgH_2 in the presence and absence of cobalt as catalyst and the most favorable reaction conditions were investigated. It was shown that the methanation mechanism depends on the presence of catalyst and its nature and other factors such as the grade of microstructural refinement, molar ratio H_2:CO_2, reaction time and temperature are crucial and non-independent factors for the process effectiveness. Without catalyst the process is favored employing a molar ratio MgH_2:CO_2 of 2:1. In this condition, a methane yield of 44.6% was obtained after 24 h of thermal treatment at 400°C. As predicted from thermodynamic calculations, the gas phase was a mixture of CH_4 and H_2. The experiments also showed the presence of small amounts of CO_2, CO and superior hydrocarbons in the gas phase, whereas the solid product contained Mg, MgO, and C with little $MgCO_3$. The global mechanism for the un-catalyzed MgH_2 involves the direct reduction of CO_2 and the generation of CH_4 *via* C as an intermediary. When either the temperature or the reaction time is lowered, the performance values drop sharply because while equilibrium is not reached, CO_2 is not totally reduced to C, but it is partially reduced to CO. Otherwise, for the MgH_2 catalyzed process the optimal molar ratio was demonstrated to be 4:1. A methane yield of 78% was achieved by heat treatment at 350 °C for 48 h. The global mechanism responds to a Sabatier process favored by Co as an active catalyst and it also involves reversed water gas shift reaction followed by methanation of CO in presence of steam. The catalyzed process is more selective, as there was no evidence of the formation of superior hydrocarbons.

It was proved that the use of catalyst allows lowering the operational temperature without reducing the methane yield. Then, this investigation provides valuable advances in research related to CO_2 methanation employing a solid hydrogen storage medium as a H_2 source.

Conflicts of interest

There are no conflicts to declare.

Acknowledgements

The present work is part of the CO2MPRISE, "CO_2 absorbing Materials Project- RISE", a project that has received funding from the European Union's Horizon 2020 research and innovation programme, under the Marie Skłodowska-Curie Grant Agreement No 734873. The work was also supported by CONICET (Consejo Nacional de Investigaciones Científicas y Técnicas), ANPCyT-(Agencia Nacional de Promoción Científica y Tecnológica) and CNEA (Comisión Nacional de Energía Atómica).

The authors also thank Bernardo Pentke (Departamento Fisicoquímica de Materiales) for the SEM micrographs, Pierre Arneodo Larochette (Departamento Fisicoquímica de Materiales) for TG measurements and Sebastian Anguiano for Raman measurements (Laboratorio de Fotónica y fotoelectrónica).

Notes and references

1. D. A. Rand, R. M. Dell. Hydrogen Energy- Challenges and Prospects. RSC Publishing: Cambridge, UK, 2008, 7-32. .

2. A. Olhoff, J. Christensen. United Nations Environment Programme (2019). Emissions Gap Report 2019. UNEP, Nairobi. Available at: http://www.unenvironment.org/emissionsgap. Accessed 1 February 2020.

3. D. Leung, G. Caramanna, M. Maroto-Valer. R*enewable Sustainable Energy Rev.*, 2014, **39**, 426.

4. M. Bui, C. Adjiman, A. Bardow, E. Anthony, A. Boston, S. Brown, P. Fennell. *Energy Environ. Sci.*, 2018, **11**, 1062.

5. M. Aresta, A. Dibenedetto, A. Angelini. *Chem. Rev.*, 2014, **114**, 1709.

6. T. Numpilai, N. Chanlek, Y. Poo-Arporn, C. K. Cheng, N. Siri-Nguan, T. Sornchamni, M. Chareonpanich, P. Kongkachuichay, N. Yigit, G. Rupprechter, J. Limtrakul, T. Witoon. Chem. Cat. Chem., 2020, https://doi.org/10.1002/cctc.202000347.

7. T. Numpilai, P. Kidkhunthod, C. K. Cheng, C. Wattanakit, M. Chareonpanich, J. Limtrakul, T. Witoon, Catalysis Today, 2020, https://doi.org/10.1016/j.cattod.2020.03.011.

8. P. Sabatier, J. B. Senderens. *Acad. Sci. Paris*, 1902, 134, 514–516.

9. C. Vogt, M. Monai, G. J. Kramer, B. M. Weckhuysen. *Nature catalysis*, 2019, **2**, 188.
10. M. Götz, J. Lefebvre, F. Mörs, A. M. D. Koch, F. Graf,S. Bajohr, R. Reimert, T. Kolb. *Renewable Energy*, 2016, **85**, 1371.
11. T. Schaaf, J. Grünig, M. Roman Schuster, T. Rothenfluh, A. Orth. *J. Energy Sustainable Soc.*, 2014, **4**, 2.
12. S. Rönsch, J. Schneider, S, Matthischke, M. Schlüter, M Götz, J. Lefebvre, P. Prabhakaran, S. Bajohr. *Fuel*, 2016, **166**, 276.
13. S. Schiebahn, T. Grube, M. Robinius, V. Tietze, B. Kumar, D. Stolten. *Int. J. of Hydrogen Energy,* 2015, **40**, 4285.
14. S. Schiebahn, T. Grube, M. Robinius, V. Tietze, B. Kumar, D. Stolten. *Renewable and Sustainable Energy Reviews*, 2017, **69**, 292.
15. D. Bessarabov, P. Millet. *Hydrogen and Fuel Cells Primers*, 2018, 95.
16. P. Frontera, A. Macario, M. Ferraro, P. L. Antonucci. *Catalysts*, 2017, **7**, 59.
17. W. Li, H. Wang, X. Jiang, J. Zhu, A. Liu, X. Guo, C. Song. *RSC Adv.*, 2018, **8**, 7651.
18. M. Younas, L. L. Kong, M. J. K. Bashir, H. Nadeem, A. Shehzad, S. Sethupathi. *Energy Fuels*, 2016, **30**, 8815.
19. S. Sahebdelfar, M. T. Ravanchi. *J. Pet. Sci. Eng.* 2015, **134**, 14.
20. X. Su, J. Xu, B. Liang, H. Duan, B. Hou, Y. Huang. *J. Energy Chem*., 2016, **25**, 553.
21. C. Lui, T. R. Cundari, A. K. Wilson. *J. Phys. Chem. C,* 2012, **116**, 5681.
22. F. Pompeo, N. N. Nichio, O. A. Feretti, D. Resasco. *Int. J. of Hydrogen energy,* 2005, **30**, 1399.
23. S. Tada, T. Shimizu, H. Kameyama, T. Haneda, R. Kikuchi. *Int. J. Hydrogen Energy,* 2012, **37**, 5527.
24. M. Guo, G. Lu. *Catal. Commun.,* 2014, **54**, 55.
25. S. Candamano, P. Frontera, A. Macario, F. Crea, N. B. Nagy. *Chem. Eng. Res. Des*., 2015, **96**, 78.
26. M. Lo Faro, P. Frontera, P. L. Antoniucci, A. S. Arico. *Chem. Eng. Res. Des.,* 2015, **93**, 269.
27. S. De, J. Zhang, R. Luque, N. Yan. *Energy Environ. Sci*., 2016, **9**, 3314.
28. X. Wang, T. Zhen, C. Yu. *Appl. Petrochem Res*., 2016, **6**, 1.
29. P. Selvam, B. Viswanathan, V. Srinivasan. *J. Less-Common Met.*, 1990, **158**, L1–L7.
30. P. Selvam, B. Viswanathan, V. Srinivas. *Int. J. Hydrogen Energy*, 1990, **15**, 133.
31. K. Kato, A. Borgschulte, D. Ferri, M. Bielmann, J-C Crivello, D. Wiedenmann, M. Parlinska-Wojtan, P. Rossbach, Y. Lu, A. Remhofa, A. Zuttel. *Phys. Chem. Chem. Phys*., 2012, **14**, 5518.
32. C. L. Hugelshofer, A. Borgschulte, E. Callini, S. K. Matam, J. Gehrig, D. Hog, A. Züttel. *J. Phys. Chem. C*, 2014, **118**, 15940.
33. J. G. Vitillo, E. Groppo, E. Gil Bardají, M. Baricco, S. Bordiga. *Phys. Chem. Chem. Phys*., 2014, **16**, 22482.
34. M. L. Grasso, J. Puszkiel, L. Fernández Albanesi, M. Dornheim, C. Pistidda, F. C. Gennari. *Phys. Chem. Chem. Phys*., 2019, **21**, 19825.
35. M. L. Grasso, J. Puszkiel, F. C. Gennari, A. Santoru, M. Dornheim, C. Pistidda. *Phys. Chem. Chem. Phys*., 2020, **22**, 1944.
36. B. X. Dong, L. Z. Wang, L. Song, J. Zhao, Y. L. Teng. *Energy Fuels*, 2016, **30**, 6620.
37. J. Zhao, Y. F. Wei, Y. L. Cai, L-Z Wang, J. Xie, Y. Teng, L. Zhu, M. Shen, B. X. *ACS Sustainable Chem. Eng*., 2019, **7**, 4831.
38. M. A. A. Aziz, A. A. Jalil, S. Triwahyono, A. Ahmad. *Green Chemistry*, 2015, **17**, 2647.
39. H. S. C. Outokumpu, Chemistry for Windows, Version 6.1, Outokumpu Research Oy, Finland, 2009.
40. H. Du, C. T. Williams, A. D. Ebner, J. A. Ritter.*Chem. Mater.,* 2010, **22**, 3519.
41. X. Jiao, H. Li, L. Li, F. Xiao, N. Zhao, W. *RSC Adv.,* 2014, **4**, 47012.
42. S. Zheng, F. Fang, J. Zhang, L. Sun, B. He, S. Wei, G. Chen, D. J. Sun. J. Phys. Chem C. 2007, **111**, 14021.
43. N. Makhoukhi, E. Péré, R. Creff, C. Pouchana. *Journal of Molecular Structure*, 2005, **744–747**, 855.
44. M. G. Verón, H. Troiani, F. C. Gennari. *Carbon*, 2011, 49, 2413.
45. M. G. Verón, F. C. Gennari, G. O. Meyer. *Journal of Power Sources*, 2010, **195**, 546.
46. G. Gao, Y. Wang, Y. Ping, D. Hu, G. Xu, F. Gu, F. Su. RSC Advance, 2012, **2**, 2358.